Structural, Thermodynamic, and Mutational Analyses of a Psychrotrophic RNase HI[†,‡]

Takashi Tadokoro,[§] Dong-Ju You,[§] Yumi Abe,[§] Hyongi Chon,[§,||] Hiroyoshi Matsumura,[⊥,@] Yuichi Koga,[§] Kazufumi Takano,[§,@] and Shigenori Kanaya*[,§]

Department of Material and Life Science and Department of Applied Chemistry, Graduate School of Engineering, Osaka University, 2-1 Yamadaoka, Suita, Osaka 565-0871, Japan, and CREST, JST, 2-1 Yamadaoka, Suita, Osaka 565-0871, Japan

Received January 24, 2007; Revised Manuscript Received March 29, 2007

ABSTRACT: Ribonuclease (RNase) HI from the psychrotrophic bacterium *Shewanella oneidensis* MR-1 was overproduced in *Escherichia coli*, purified, and structurally and biochemically characterized. The amino acid sequence of MR-1 RNase HI is 67% identical to that of *E. coli* RNase HI. The crystal structure of MR-1 RNase HI determined at 2.0 Å resolution was highly similar to that of *E. coli* RNase HI, except that the number of intramolecular ion pairs and the fraction of polar surface area of MR-1 RNase HI were reduced compared to those of *E. coli* RNase HI. The enzymatic properties of MR-1 RNase HI were similar to those of *E. coli* RNase HI. However, MR-1 RNase HI was much less stable than *E. coli* RNase HI. The stability of MR-1 RNase HI against heat inactivation was lower than that of *E. coli* RNase HI by 19 °C. The conformational stability of MR-1 RNase HI was thermodynamically analyzed by monitoring the CD values at 220 nm. MR-1 RNase HI was less stable than *E. coli* RNase HI by 22.4 °C in T_m and 12.5 kJ/mol in $\Delta G(H_2O)$. The thermodynamic stability curve of MR-1 RNase HI was characterized by a downward shift and increased curvature, which results in an increased ΔC_p value, compared to that of *E. coli* RNase HI. Site-directed mutagenesis studies suggest that the difference in the number of intramolecular ion pairs partly accounts for the difference in stability between MR-1 and *E. coli* RNases HI.

Shewanella oneidensis MR-1 is a dissimilatory metal-reducing bacterium, which was isolated from sediments of Lake Oneida in the state of New York (*1*). Because of its diverse respiratory capabilities, which are conferred in part by multicomponent and branched electron transport systems, *S. oneidensis* MR-1 is considered as an important candidate for bioremediation studies. Therefore, its whole genome sequence has been completely determined as a model organism for the development of bioremediation strategies (GenBank entry NC_004347) (*2*). This bacterium was originally identified as a mesophile, because its optimum growth temperature is around 30 °C. However, it has recently been shown that this bacterium can grow even at temperatures near 0 °C (*3*). According to the revised definition of Morita and Moyer (*4*), this bacterium is a psychrotroph, instead of a mesophile.

Ribonuclease H (RNase H,[1] EC 3.1.26.4) specifically degrades the RNA strand of RNA−DNA hybrids (*5*). The enzyme is widely present in various organisms (*6*). Of them, prokaryotic RNase H has been used as a model protein to analyze stabilization mechanism of proteins. These proteins are suitable for this purpose, because they are monomeric, relatively small in size, and generally reversible in thermal and chemical denaturation. Studies of the stabilization mechanism of *Escherichia coli* RNase HI indicate that limited regions in this protein molecule are not locally optimized with respect to stability, and these weak points can be reinforced by introducing favorable interactions or eliminating unfavorable interactions by the mutations (*7*). Studies of the stabilization mechanism of RNase HII from the hyperthermophilic archaeon *Thermococcus kodakaraensis* indicate that this protein is characterized by remarkably slow unfolding (*8*). Studies on the stabilization mechanism of RNase HI from the extremely thermophilic bacterium *Thermus thermophilus* indicate that this protein is characterized by a lower ΔC_p (change in heat capacity upon unfolding) (*9*).

Psychrophiles and psychrotrophs usually produce cold-adapted enzymes, which are specified by an increase in the

[†] This work was supported in part by a Grant-in-Aid for National Project on Protein Structural and Functional Analyses and by a Grant-in-Aid for Scientific Research on Priority Areas "Systems Genomics" from the Ministry of Education, Culture, Sports, Science, and Technology of Japan, and by an Industrial Technology Research Grant Program from the New Energy and Industrial Technology Development Organization (NEDO) of Japan.

[‡] The Protein Data Bank entry for MR-1 RNase HI is 2E4L.

* To whom correspondence should be addressed. Telephone and fax: +81-6-6879-7938. E-mail: kanaya@mls.eng.osaka-u.ac.jp.

[§] Department of Material and Life Science, Graduate School of Engineering, Osaka University.

[||] Present address: Laboratory of Molecular Genetics, National Institutes of Health, Bethesda, MD 20892.

[⊥] Department of Applied Chemistry, Graduate School of Engineering, Osaka University.

[@] CREST.

[1] Abbreviations: RNase H, ribonuclease H; CD, circular dichroism; GdnHCl, guanidine hydrochloride; H8E/N29R/T34E, mutant protein of MR-1 RNase HI, in which His8, Asn29, and Thr34 are replaced with Glu, Arg, and Glu, respectively.

10.1021/bi7001423 CCC: $37.00 © 2007 American Chemical Society
Published on Web 05/31/2007

catalytic efficiency at low temperatures, a downward shift in the apparent optimum temperature for activity, and a reduction in stability at moderate temperatures, as compared to those of its mesophilic counterpart (*10*−*13*). The molecular basis for cold adaptation, however, remains largely unknown. One of the promising strategies for analyzing the cold adaptation mechanism of enzymes is to compare the structure and function of a given enzyme from psychrophiles or psychrotrophs with those of the mesophilic counterpart and identify the amino acid substitutions responsible for these differences. For this purpose, we have previously cloned the gene encoding RNase HI from the psychrotrophic bacterium *Shewanella* sp. SIB1 and biochemically characterized the recombinant protein (*14*). SIB1 RNase HI exhibits features typical of cold-adapted enzymes. However, this protein is not suitable as a partner of *E. coli* RNase HI for analysis of the cold adaptation mechanism of proteins, because it is irreversible in thermal and chemical denaturation.

In this study, RNase HI from the psychrotrophic bacterium *S. oneidensis* MR-1 was overproduced in *E. coli*, purified, and structurally and biochemically characterized. The crystal structure and enzymatic properties of this protein were highly similar to those of *E. coli* RNase HI. Nevertheless, MR-1 RNase HI was thermodynamically much less stable than *E. coli* RNase HI. Mutational studies suggest that the decreased number of ion pairs is one of the factors responsible for the thermolability of MR-1 RNase HI.

MATERIALS AND METHODS

Purification of the Protein. Plasmid pET500M for overproduction of MR-1 RNase HI was constructed by ligating the 500 bp DNA fragment into the *Nde*I−*Sal*I sites of pET25b (Novagen). This DNA fragment was amplified by PCR using the genomic DNA of *S. oneidensis* MR-1, which was kindly donated by R. Colter, as a template. The sequences of the PCR primers are 5′-CGCTATGGTAACAACCATATGACTGAACTA-3′ for the 5′ primer and 5′-GCGCGTCGACTTAAGACTCCGCCTGATAGCCAGT-3′ for the 3′ primer, where underlined bases show the positions of the *Nde*I and *Sal*I sites. The DNA sequence was confirmed with a Prism 310 DNA sequencer (Perkin-Elmer).

Overproduction of MR-1 RNase HI using the transformants of an RNase H-deficient mutant strain, *E. coli* MIC2067(DE3), with pET500M was carried out as described for *Shewanella* sp. SIB1 RNase HI (*14*). Cells were harvested by centrifugation at 8000 rpm for 10 min, suspended in 10 mM Tris-HCl (pH 7.5) containing 1 mM EDTA, disrupted by sonication lysis, and centrifuged at 30000*g* for 30 min. The supernatant was applied to a cation-exchange column (3 mL) of P-11 (Whatman) equilibrated with 10 mM Tris-HCl (pH 7.5). After the column had been washed, the protein was eluted from the column with a linear gradient of NaCl from 0 to 1.0 M in the same buffer. The fractions containing the protein were pooled, dialyzed against 10 mM Tris-HCl (pH 7.5), and applied to a Hitrap Heparin HP column (Amersham Biosciences) equilibrated with the same buffer. After the column had been washed, the protein was eluted from the column with a liner gradient of NaCl from 0 to 1 M in the same buffer. The fractions containing the protein were pooled and dialyzed against 10 mM sodium acetate (pH 5.5). *E. coli* RNase HI was overproduced and purified as described previously (*15*). The purity of the protein was analyzed by SDS−PAGE using a 15% polyacrylamide gel (*16*), followed by staining with Coomassie Brilliant Blue.

The protein concentration was determined from the UV absorption on the basis that the absorbance at 280 nm of a 0.1% solution is 2.1 for MR-1 RNase HI and 2.0 for *E. coli* RNase HI. These values were calculated by using an ϵ of 1576 M^{-1} cm^{-1} for Tyr and an ϵ of 5225 M^{-1} cm^{-1} for Trp at 280 nm (*17*).

Crystallization. MR-1 RNase HI was concentrated using an ultrafiltration Centricon system (Millipore) to 8−12 mg/mL. The crystallization conditions were initially screened using crystallization kits from Hampton Research (Crystal Screens I and II) and Emerald Biostructrues (Wizard I and II). The conditions were surveyed using the sitting-drop vapor-diffusion method at 4 °C. Drops were prepared by mixing 1 μL each of the protein and reservoir solutions and were vapor-equilibrated against 100 μL of reservoir solution. Native crystals of MR-1 RNase HI suitable for X-ray diffraction analysis appeared after 3 weeks using Wizard II solution No. 19 [1.6 M NaH_2PO_4, 0.4 M K_2HPO_4, and Tris-HCl (pH 7.0)].

X-ray Diffraction Data Collection and Structure Determination. X-ray diffraction data sets of the MR-1 RNase HI crystal were collected at 100 K using synchrotron radiation on the BL44XU station at SPring-8, using a DIP6040 multiple-imaging plate diffractometer. These data sets were processed with HKL2000 (*18*). The crystal structure was determined via the molecular replacement method using MOLREP (*19*) in the CCP4 program suite. The refined 1.48 Å structure of *E. coli* RNase HI (PDB entry 2RN2) was used as a starting model. Model building and refinement of the structures were completed using COOT (*20*) and REFMAC (*21*) in the CCP4 program suite. Progress in the structure refinement was evaluated at each stage by R_{free} and by inspection of stereochemical parameters calculated with PROCHECK (*22*). The Ramachandran plot produced by PROCHECK shows that 100% of the residues in the structure fall in the most favored and allowed regions. The statistics for data collection and refinement are summarized in Table 1. The figures were prepared with RasMol (*23*).

The number of ion pairs in the crystal structure was calculated on the basis of the assumption that an ion pair is formed between two oppositely charged residues located within 5 Å of each other. This distance was calculated using *CONTACT* from the CCP4 program package (*24*). The electrostatic surface potential of the protein was calculated using GRASP (*25*), with potentials ranging from −15 to 15 kT/e. The solvent accessible surface area (ASA) of the protein was calculated using ACCESS with a probe radius of 1.4 Å.

Protein Data Bank Entry. The coordinates and structure factors of MR-1 RNase HI have been deposited in the Protein Data Bank as entry 2E4L.

Mutagenesis. The gene encoding the mutant protein H8E/N29R/T34E was constructed by site-directed mutagenesis using PCR, as described previously (*14*). For PCR, plasmid pET500M was used as a template. The mutagenetic primers were designed such that the codons for His8 (CAC), Asn29 (AAT), and Thr34 (ACA) are changed to those for Glu (GAG), Arg (AGA), and Glu (GAA), respectively. The nucleotide sequence of the gene encoding the mutant protein

Table 1: Data Collection and Refinement Statistics

Data Collection	
beamline	BL44XU
wavelength (Å)	0.90
resolution (Å)	50−1.80 (1.86−1.80)
no. of observations	180769
no. of unique reflections	21823
completeness (%)	99.7 (98.3)
R_{merge} (%)[a]	6.6 (39.0)
average $I/\sigma(I)$	37.8 (5.1)
Refinement	
resolution limit (Å)	27.2−2.0
space group	*P*422
unit cell	$a = b = 77.1$ Å, $c = 76.7$ Å $\alpha = \beta = \gamma = 90°$
no. of molecules	1
no. of protein atoms	1223
no. of waters	169
R-factor (%)	19.0
R_{free} (%)[b]	21.8
rmsd	
bond lengths (Å)	0.035
bond angles (deg)	2.3
mean *B*-factor (Å^2)	
main chain	23.89
side chain	28.77

[a] $R_{merge} = \sum|I_{hkl} - \langle I_{hkl}\rangle|/\sum I_{hkl}$, where I_{hkl} is the intensity measurement for a reflection with indices *hkl* and $\langle I_{hkl}\rangle$ is the mean intensity for multiply recorded reflections. [b] R_{free} was calculated using 5% of the total reflections chosen randomly and omitted from refinement.

was confirmed by using a Prism 310 DNA sequencer (Applied Biosystems). Overproduction and purification of the mutant protein were carried out as described for the wild-type protein. The protein concentration was determined from the UV absorption on the assumption that the absorption coefficient is not changed by the mutation.

Enzymatic Activity. The RNase H activity was determined at 30 °C and pH 8.0 by measuring the radioactivity of the acid-soluble digestion product from a ^{3}H-labeled M13 DNA−RNA hybrid, as described previously (*15*). The reaction mixture contained 10 pmol of the substrate and an appropriate amount of enzyme in 20 μL of 10 mM Tris-HCl (pH 8.0) containing 10 mM $MgCl_2$, 50 mM NaCl, 1 mM 2-mercaptoethanol (2-Me), and 50 μg/mL BSA. One unit is defined as the amount of enzyme producing 1 μmol of acid-soluble material per minute. The specific activity was defined as the enzymatic activity per milligram of protein. For determination of the kinetic parameters, the substrate concentration was varied from 0.05 to 1.0 μM. The hydrolysis of the M13 DNA−RNA hybrid by the enzyme followed Michaelis−Menten kinetics, and the kinetic parameters were determined from the Lineweaver−Burk plot.

Circular Dichroism (CD) Spectra. The CD spectra were measured on a J-725 spectropolarimeter (Japan Spectroscopic) at 4 or 60 °C. The protein was dissolved in 10 mM sodium acetate (pH 5.5) containing 5 M urea, 1 M guanidine hydrochloride (GdnHCl), or no denaturants. The protein concentration and optical path length were 0.1−0.2 mg/mL and 2 mm for far-UV CD spectra and 0.9−1.0 mg/mL and 10 mm for near-UV CD spectra, respectively. The mean residue ellipticity, θ, which has the units of degrees square centimeters per decimole, was calculated by using an average amino acid molecular weight of 110.

Thermal Denaturation. Thermal denaturation curves of MR-1 and *E. coli* RNases HI were obtained by monitoring the change in CD values at 220 nm as the temperature was increased. The proteins were dissolved in 10 mM sodium acetate (pH 5.5) containing 1 M GdnHCl. The protein concentration and optical path length were 0.15 mg/mL and 2 mm, respectively. The temperature of the protein solution was linearly increased by approximately 1.0 °C/min. The thermal denaturations of these proteins were reversible under this condition. The temperature of the midpoint of the transition, T_m, was calculated from curve fitting of the resultant CD values versus temperature data on the basis of a least-squares analysis. The enthalpy (ΔH_m) and entropy (ΔS_m) changes for thermal denaturation at T_m were calculated by van't Hoff analysis.

Urea-Induced Denaturation. Urea denaturation curves of MR-1 and *E. coli* RNases HI were obtained by monitoring the change in CD values at 220 nm, which was measured using a cuvette with an optical path length of 2 mm. The proteins (0.15 mg/mL) were dissolved in 10 mM sodium acetate (pH 5.5) containing 100 mM NaCl and the appropriate concentrations of urea. The protein solution was incubated for at least 2 h at the indicated temperatures before the measurement. The urea denaturations of these proteins were fully reversible. On the assumption that the unfolding equilibria of these proteins follow a two-state mechanism, the pre- and post-transition baselines were extrapolated linearly, and the difference in free energy between the folded and unfolded states, ΔG, and the free energy change of unfolding in H_2O, $\Delta G(H_2O)$, were calculated via the equations given by Pace (*26*).

RESULTS

Overproduction, Purification, and Crystallization of MR-1 RNase HI. Upon induction for overproduction of MR-1 RNase HI at 30 °C, most of the recombinant protein accumulated in the cells in a soluble form. The protein was purified to give a single band on SDS−PAGE (data not shown), concentrated to 8−12 mg/mL, and used for crystallization. The crystals of cubic habit suitable for X-ray diffraction analysis appeared after 3 weeks.

Crystal Structure of MR-1 RNase HI. The crystal of MR-1 RNase HI belongs to primitive tetragonal space group *P*422, with the following unit cell parameters: $a = b = 77.1$ Å, and $c = 76.7$ Å. On the basis of the molecular weight and the space group, it was assumed that the crystal contains one protein molecule per asymmetric unit. The crystal structure was determined by molecular replacement using the *E. coli* RNase HI structure as the starting model. The final structure was refined to an *R*-factor of 19.0% and an R_{free} of 21.8% at 2.0 Å resolution. The data collection and refinement statistics are summarized in Table 1. Residues 1−3 are missing in this structure probably due to disorder.

The overall structure of MR-1 RNase HI is quite similar to that of *E. coli* RNase HI, with a root-mean-square deviation (RMSD) of 1.7 Å over 140 Cα atoms (Figure 1A). No significant difference was observed in the steric configurations of the four acidic active site residues between MR-1 and *E. coli* RNases HI. However, the MR-1 RNase HI structure is different from the *E. coli* RNase HI structure in the number of the intramolecular ion pairs, which is seven for MR-1 RNase HI and ten for *E. coli* RNase HI (Figure 1B and Table 2). Four of the seven ion pairs of MR-1 RNase

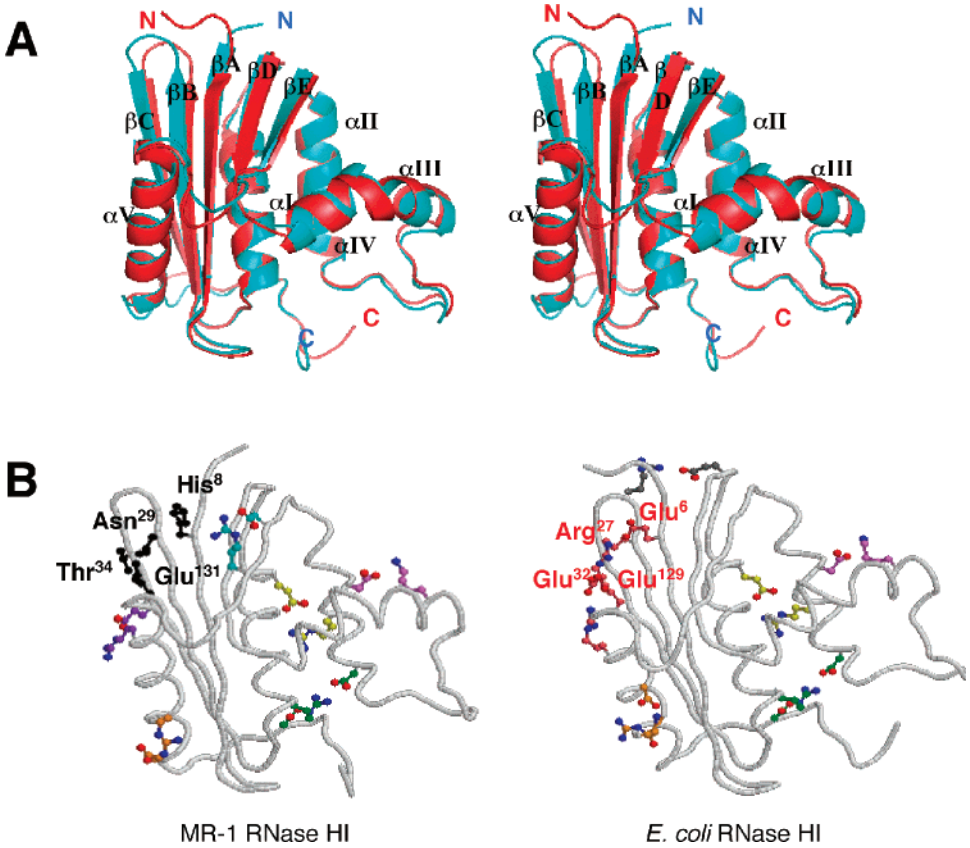

FIGURE 1: Comparison of the crystal structures of MR-1 and *E. coli* RNases HI. (A) Stereoview of the main chain folds of MR-1 RNase HI (blue) and *E. coli* RNase HI (red) superimposed. The PDB entry for *E. coli* RNase HI is 2RN2. (B) Localization of the ion pairs at the protein surface. The side chains of the amino acid residues forming ion pairs are shown as ball-and-stick models with the RNase HI backbones drawn as trace models. The ion pairs located at different positions are colored differently. Nitrogen and oxygen atoms are colored blue and red, respectively.

Table 2: Intramolecular Ion Pairs (≤5.0 Å)[a]

MR-1 RNase HI		*E. coli* RNase HI	
pair	distance (Å)	pair	distance (Å)
Glu36−Arg134	2.8	Glu6−Arg27	3.0
Glu59−Arg108	2.9	Glu32−Arg27	3.0
Asp104−Arg48	3.0	Glu32−Arg132	2.7
Asp110−Lys88	3.1	Glu57−Arg106	2.7
Asp119−Arg121	2.8	Glu61−Arg29	4.0
Glu144−Arg140	3.3	Asp102−Arg46	2.9
Asp151−Arg48	2.7	Asp108−Lys86	3.4
		Glu129−Arg27	2.6
		Asp134−Arg138	3.2
		Asp148−Arg46	2.5

[a] Conserved ion pairs are underlined.

Table 3: Comparison of the Structural Features of MR-1 and *E. coli* RNases HI

	MR-1 RNase HI	*E. coli* RNase HI
no. of atoms	1223	1238
no. of surface atoms	636	638
no. of ion pairs	7	10
ASA_{total} (Å^2)[a]	8798	8993
ASA_{pol} (Å^2)[a]	4359	4698
ASA_{np} (Å^2)[a]	4439	4295
fraction of ASA_{np}	0.505	0.478

[a] ASA was calculated using a probe radius of 1.4 Å and analyzed for polar (N and O) and nonpolar (C and S) atoms.

HI are conserved in *E. coli* RNase HI. The electrostatic surface potential of MR-1 RNase HI is similar to that of *E. coli* RNases HI but is less negative than that of *E. coli* RNase HI at the region in which the C-terminal region of the βB strand interacts with βA, βC, and αV (data not shown). The accessible surface areas for total atoms (ASA_{total}), polar atoms (ASA_{pol}), and nonpolar atoms (ASA_{np}) are summarized in Table 3. The ASA_{total} value of MR-1 RNase HI (8798 Å^2) is comparable to that of *E. coli* RNase HI (8992 Å^2). However, the fraction of nonpolar surface area (ASA_{np}/ASA_{total}) of MR-1 RNase HI is significantly larger than that of *E. coli* RNase HI.

The amino acid sequence of MR-1 RNase HI is compared with those of SIB1, *E. coli*, and *T. thermophilus* RNases HI on the basis of the crystal structure in Figure 2. The amino acid sequence of MR-1 RNase HI is 79% identical to that of SIB1 RNase HI, 67% identical to that of *E. coli* RNase HI, and 45% identical to that of *T. thermophilus* RNase HI.

Enzymatic Activity. MR-1 RNase HI exhibited the maximal activity for the hydrolysis of the M13 DNA−RNA hybrid at pH 8.0 in the presence of 10 mM $MgCl_2$ and 50 mM NaCl. The optimum pH and metal ion dependency of MR-1 RNase HI were similar to those of *E. coli* RNase HI (data not shown). Comparison of the kinetic parameters of MR-1 RNase HI with those of *E. coli* RNase HI indicates that the hydrolysis rate and substrate binding affinity of MR-1 RNase HI are comparable to those of *E. coli* RNase HI (Table 4).

Optimum Temperature for Activity. The amount of acid-soluble digestion products that accumulated upon incubation of the M13 DNA−RNA hybrid with MR-1 or *E. coli* RNase HI for 15 min was plotted as a function of temperature

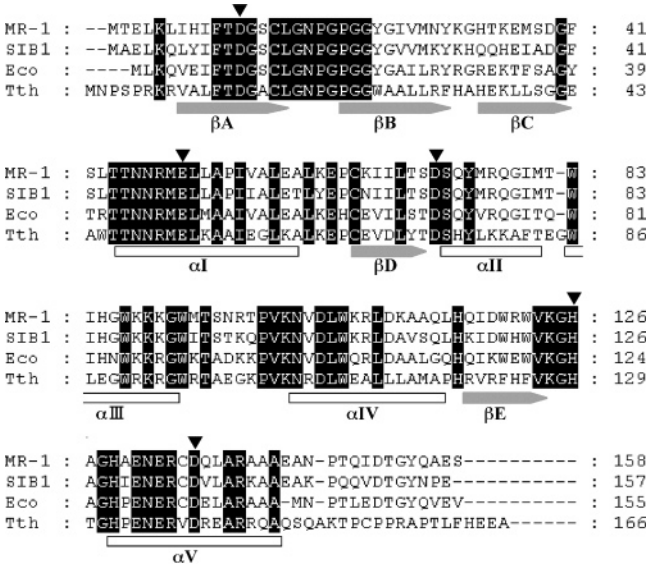

FIGURE 2: Alignment of amino acid sequences. The amino acid sequences of MR-1 RNase HI (MR-1), SIB1 RNase HI (SIB1), *E. coli* RNase HI (Eco), and *T. thermophilus* RNase HI (Tth) are shown (GenBank accession numbers NP_718146 for MR1, AB070445 for SIB1, V00337 for Eco, and X60507 for Tth). The MR-1 RNase HI, *E. coli* RNase HI, and *T. thermophilus* RNase HI sequences are aligned on the basis of a comparison of their crystal structures. The ranges of the secondary structures of MR-1 RNase HI are shown below the sequences. The positions of the four acidic active site residues are denoted with triangles (▼). The amino acid residues that are conserved in all four proteins are highlighted in black. Gaps are denoted by dashes. The numbers represent the positions of the amino acid residues relative to the initiator methionine for each protein.

(Figure 3). As long as these amounts were compared with one another, MR-1 and *E. coli* RNases HI most effectively hydrolyzed the substrate at 45 and 55 °C, respectively, indicating that the optimum temperature for activity of MR-1 RNase HI is lower than that of *E. coli* RNase HI by 10 °C.

Stability against Heat Inactivation. The stabilities of MR-1 and *E. coli* RNases HI against irreversible heat inactivation were analyzed by incubating the protein in 20 mM Tris-HCl (pH 7.5) containing 0.1 M KCl, 1 mM EDTA, 10% glycerol, and 0.1 mg/mL BSA at various temperatures for 10 min and measuring the residual activity at 30 °C (Figure 4). The temperature ($T_{1/2}$) at which the enzyme loses half of its activity was approximately 36 °C for MR-1 RNase HI and 55 °C for *E. coli* RNase HI, indicating that MR-1 RNase HI is less stable than *E. coli* RNase HI by 19 °C in $T_{1/2}$.

Stability against Thermal Denaturation. The far- and near-UV CD spectra of MR-1 RNase HI recorded under various conditions are shown in Figure 5. The spectra measured at 4 °C in the presence or absence of 1 M GdnHCl represent those of the protein in a native state, while those measured at 60 °C or in the presence of 5 M urea represent those of the protein in a denatured state. The thermal denaturation curve of MR-1 RNase HI was measured at pH 5.5 in the presence of 1.0 M GdnHCl and compared with that of *E. coli* RNase HI in Figure 6. Thermal denaturation of these proteins is almost fully reversible under this condition. The thermodynamic parameters characterizing the thermal denaturation curves of MR-1 and *E. coli* RNases HI are summarized in Table 4. The temperature of the midpoint of the transition, T_m, was 30.4 °C for MR-1 RNase HI and 52.8 °C for *E. coli* RNase HI. Thus, MR-1 RNase HI is less stable than *E. coli* RNase HI by 22.4 °C in T_m.

To determine the T_m values of MR-1 and *E. coli* RNases HI in the absence of GdnHCl, in which thermal denaturation of these proteins is not reversible, the thermal denaturation curves of these proteins were measured in the presence of various concentrations (0.5−1.0 M) of GdnHCl (Figure 7). Thermal denaturation of these proteins is highly reversible under these conditions. Because the T_m values of both proteins increased in proportion to a decrease in GdnHCl concentration, the T_m values of these proteins in the absence of GdnHCl were estimated to be 53.2 °C for MR-1 RNase HI and 70.7 °C for *E. coli* RNase HI by the linear extrapolation. These values were comparable to the midpoints of the transition of the thermal denaturation curves determined in the absence of GdnHCl, which were 52.7 °C for MR-1 RNase HI and 71.7 °C for *E. coli* RNase HI (data not shown).

Stability against Urea-Induced Denaturation. To estimate the difference in the apparent free energy change of unfolding in the absence of denaturant, $\Delta G(H_2O)$, between MR-1 and *E. coli* RNases HI, the urea-induced denaturation curves of these proteins were measured at pH 5.5 and 20 °C by monitoring the change in the CD values at 220 nm, as shown in Figure 8. Urea-induced denaturation of these proteins is fully reversible under this condition, and both proteins exhibit a two-state transition. The thermodynamic parameters characterizing the urea-induced denaturation curves of MR-1 and *E. coli* RNases HI are summarized in Table 4. The $\Delta G(H_2O)$ value and the midpoint of the denaturation curve, C_m, of MR-1 RNase HI were lower than those of *E. coli* RNase HI by 12.5 kJ/mol and 1.67 M, respectively.

Temperature Dependence of $\Delta G(H_2O)$. The urea-induced denaturation curves were measured at various temperatures ranging from 4 to 25 °C for MR-1 RNase HI and from 10 to 30 °C for *E. coli* RNase HI (Figure 9), and the $\Delta G(H_2O)$ value at each temperature was calculated. The resultant $\Delta G(H_2O)$ values were plotted as a function of temperature (Figure 10). These plots include a $\Delta G(H_2O) = 0$ plot at T_m, which was estimated from the thermal denaturation experiment mentioned above (53.2 °C for MR-1 RNase HI and 70.7 °C for *E. coli* RNase HI). These data were fit to the Gibbs−Helmholtz equation:

$$\Delta G(H_2O) = \Delta H_m - T\Delta H_m/T_m + \Delta C_p[T - T_m - T\ln(T/T_m)] \quad (1)$$

to calculate ΔH_m and ΔC_p. ΔH_m is the enthalpy change of unfolding at T_m, and ΔC_p is the difference in heat capacity between the native and unfolded states. The resultant ΔH_m and ΔC_p values were used to calculate T_s, $\Delta G(T_s)$, and $\Delta G(T_L)$. T_s is the temperature at which the protein exhibits the maximal $\Delta G(H_2O)$ value; $\Delta G(T_s)$ is the $\Delta G(H_2O)$ value at T_s, and $\Delta G(T_L)$ is the $\Delta G(H_2O)$ value at the optimum growth temperature of the source organism. All of these thermodynamic parameters are summarized in Table 4. The ΔC_p and ΔH_m values of MR-1 RNase HI were lower than those of *E. coli* RNase HI by 3.38 kJ mol^{-1} K^{-1} and 37.4 kJ/mol, respectively. The $\Delta G(T_L)$ value of MR-1 RNase HI was lower than that of *E. coli* RNase HI by 11.4 kJ/mol.

Stability of H8E/N29R/T34E. To examine whether MR-1 RNase HI is stabilized via introduction of an ion pair

Table 4: Comparison of the Enzymatic Activities and Stabilities of MR-1 and *E. coli* RNase HI

	MR-1 RNase HI	H8E/N29R/T34E	*E. coli* RNase HI
enzymatic activity[a]			
specific activity (units/mg)	7.8	7.9	9.1
K_m (μM)	0.30	ND	0.11
V_{max} (units/mg)	8.6	ND	9.5
parameters characterizing thermal denaturation[b]			
T_m (°C)	30.4 ± 0.8	36.0 ± 1.2	52.8 ± 0.9
ΔH_m (kJ/mol)	217 ± 14	235 ± 10	325 ± 12
ΔS_m (kJ mol^{-1} K^{-1})	0.72 ± 0.03	0.77 ± 0.05	1.0 ± 0.06
parameters characterizing urea-induced denaturation[c]			
C_m (M)	2.6 ± 0.2	3.2 ± 0.2	4.3 ± 0.3
m (kJ mol^{-1} M^{-1})	8.5 ± 0.8	8.5 ± 0.7	8.2 ± 0.4
$\Delta G(H_2O)$ (kJ/mol)	22.3 ± 1.8	27.0 ± 1.9	34.8 ± 2.3
$\Delta\Delta G(H_2O)$ (kJ/mol)[d]	−	4.7	12.5
thermodynamic parameters[e]			
T_m (°C)	53.2 ± 0.5	ND	70.7 ± 1.0
ΔC_p (kJ mol^{-1} K^{-1})	11.9 ± 1.4	ND	8.1 ± 1.1
ΔH_m (kj/mol)	418 ± 15	ND	455 ± 18
T_s (°C)	18.3	ND	19.9
$\Delta G(T_s)$ (kJ/mol)	22.5	ND	35.1
$\Delta G(T_L)$ (kJ/mol)	19.8 (at 30 °C)	ND	31.2 (at 37 °C)

[a] Specific activities and kinetic parameters were determined at 30 °C using the M13 DNA−RNA hybrid as a substrate. Errors, which represent the 67% confidence limits, are all at or below ±20% of the values reported. [b] These values were determined from the thermal denaturation curves of the proteins obtained at pH 5.5 in the presence of 1 M GdnHCl with a scan rate of 1 °C/min. The experiment was carried out in duplicate. The average values and the errors from them are indicated. [c] These values were determined from the urea-induced denaturation curves of the proteins obtained at 20 °C. The experiment was carried out in duplicate. The average values and the errors from them are indicated. [d] $\Delta G(H_2O)$ of *E. coli* RNase HI or H8E/N29R/T34E − $\Delta G(H_2O)$ of MR-1 RNase HI. [e] These values were determined from the protein stability curves shown in Figure 10. T_m, ΔC_p, and ΔH_m were determined from fits of the protein stability curves to the Gibbs−Helmholtz equation (eq 1). T_s is the temperature of maximal stability, $\Delta G(T_s)$ the maximal stability, and $\Delta G(T_L)$ the stability at the optimum growth temperature of the source organism. The experiment was carried out in duplicate. The average values and the errors from them are indicated.

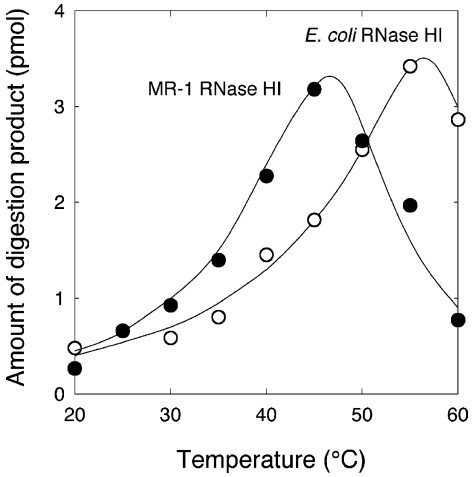

FIGURE 3: Temperature dependencies of the enzymatic activities of MR-1 and *E. coli* RNases HI. The M13 DNA−RNA hybrid was hydrolyzed by 20 pg of MR-1 RNase HI or 10 pg of *E. coli* RNase HI at the temperatures indicated in 20 μL of the reaction mixture, and the amount of acid-soluble digestion products that accumulated upon enzymatic reaction was plotted as a function of temperature.

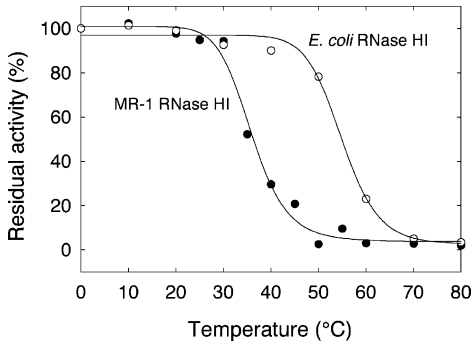

FIGURE 4: Stability against irreversible heat inactivation. The enzyme was dissolved in 20 mM Tris-HCl (pH 7.5) containing 0.1 M KCl, 1 mM EDTA, 10% glycerol, and 0.1 mg/mL BSA at a concentration of 0.02−0.3 μg/mL and incubated for 10 min at the indicated temperatures, and the residual activities were determined at 30 °C using the M13 DNA−RNA hybrid as a substrate.

network, which is not present in the MR-1 RNase HI structure but is present in the *E. coli* RNase HI structure, the mutant protein H8E/N29R/T34E was constructed. This mutant protein is expected to have an ion pair network at the region, where Glu6, Arg27, Glu32, and Glu129 form an ion pair network in the *E. coli* RNase HI structure (Figure 1B). H8E/N29R/T34E was overproduced in *E. coli* and purified, as was the wild-type protein. Its specific activity was nearly identical to that of the wild-type protein (Table 4), suggesting that the mutations do not seriously affect the protein structure. Comparison of the thermal denaturation curves of the mutant and wild-type proteins (Figure 6) indicates that the mutant protein is more stable than the wild-type protein by 5.6 °C in T_m. Likewise, comparison of the urea-induced denaturation curves of the mutant and wild-type proteins (Figure 8) indicates that the mutant protein is more stable than the wild-type protein by 4.7 kJ/mol in $\Delta G(H_2O)$.

DISCUSSION

Importance of Ionic Interactions for Protein Stability. The structural features of cold-adapted enzymes have been reported to be a reduced number of ion pairs, a reduced number of hydrophobic interactions at the core, an increased fraction of nonpolar surface area, and a reduced number of the proline residues in the loop regions (*10*−*13*). However, the structures of cold-adapted enzymes are not always characterized by the reduced number of ion pairs (*27*) and

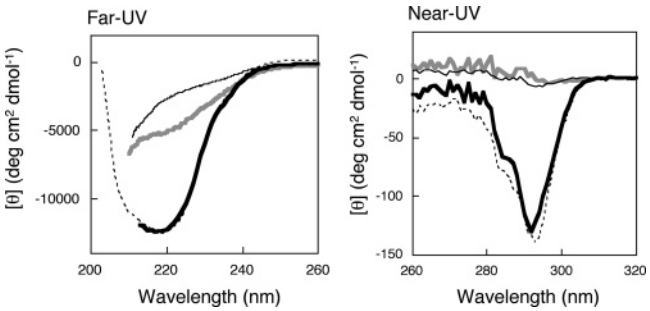

FIGURE 5: Far-UV and near-UV CD spectra of MR-1 RNase HI. The spectra were measured at pH 5.5 and 4 °C in the presence of 1 M GdnHCl (thick solid line) or 5 M urea (thin solid line) or in the absence of these denaturants (dashed line). The spectra were also measured at pH 5.5 and 60 °C in the presence of 1 M GdnHCl (gray line).

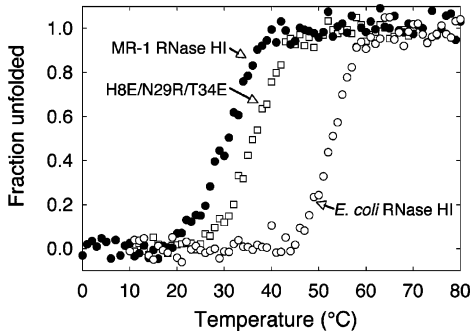

FIGURE 6: Thermal denaturation curves of MR-1 RNase HI, H8E/N29R/T34E, and *E. coli* RNase HI. These curves were recorded at pH 5.5 in the presence of 1.0 M GdnHCl by monitoring the change in the CD value at 220 nm as described in Materials and Methods.

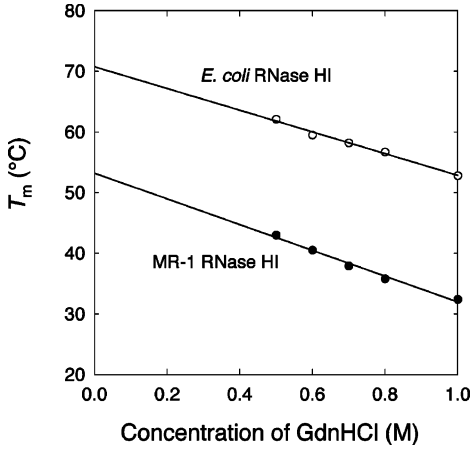

FIGURE 7: Dependence of T_m on GdnHCl concentration. The T_m values of MR-1 and *E. coli* RNases HI determined at pH 5.5 in the presence of various concentrations of GdnHCl ranging from 0.5 to 1.0 M are plotted as a function of the GdnHCl concentration. The lines represent a linear fit of the data. Thermal denaturation of both proteins was almost fully reversible under these conditions.

an increased fraction of nonpolar surface area (*28*). Thus, the strategies for cold adaptation vary for different proteins.

When the crystal structure of MR-1 RNase HI is compared with that of *E. coli* RNase HI, a significant difference is detected in the ionic interactions at the molecular surface, especially for the region in which the C-terminal region of the βB strand interacts with βA, βC, and αV (Figure 1B). In the *E. coli* RNase HI structure, Glu6, Arg27, Glu32, and Glu129 form ion pairs in this region. In the MR-1 RNase HI structure, however, these ion pairs are missing, because

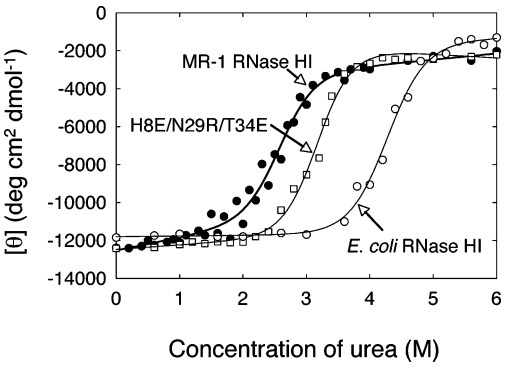

FIGURE 8: Urea-induced denaturation curves of MR-1 RNase HI, H8E/N29R/T34E, and *E. coli* RNase HI at 20 °C. The CD value at 220 nm is shown as a function of urea concentration. The methods are described in Materials and Methods. The theoretical curves are drawn on the assumption that the proteins are denatured via a two-state mechanism.

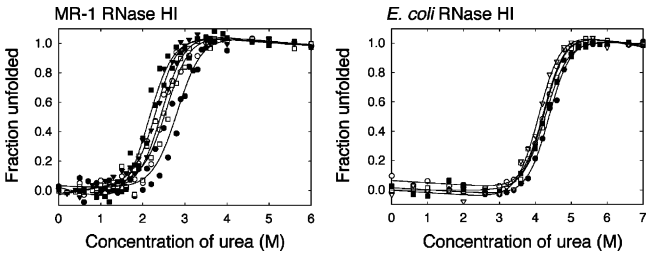

FIGURE 9: Urea-induced denaturation curves of MR-1 and *E. coli* RNases HI at various temperatures. The apparent fraction of denatured protein is shown as a function of temperature: (▼) 4, (○) 10, (●) 15, (□) 20, (■) 25, and (▽) 30 °C. The theoretical curves are drawn on the assumption that the proteins are denatured via a two-state mechanism.

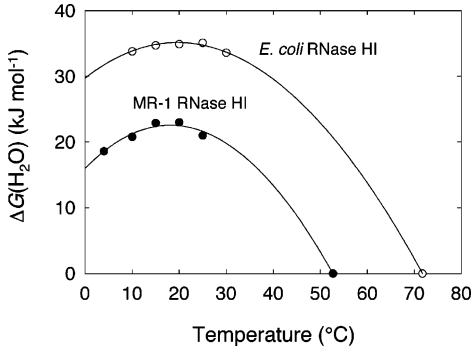

FIGURE 10: Thermodynamic stability profiles of MR-1 and *E. coli* RNases HI. The $\Delta G(H_2O)$ values of the proteins determined from an equilibrium experiment are shown as a function of temperature. The T_m values, at which the $\Delta G(H_2O)$ values become zero, were estimated to be 53.2 °C for MR-1 RNase HI and 70.7 °C for *E. coli* RNase HI from Figure 7. Lines represent fits to the Gibbs−Helmholtz equation (eq 1).

Glu6, Arg27, and Glu32 are replaced with His8, Asn29, and Thr34, respectively. The qualitative evaluation of the electrostatic surface potentials of MR-1 and *E. coli* RNases HI also indicates that the negative charge density of MR-1 RNase HI is lower than that of *E. coli* RNase HI in this region (data not shown). Therefore, a reduction in the number of ion pairs is probably responsible for the thermolability of MR-1 RNase HI. In fact, the observation that the triple mutant protein of MR-1 RNase HI, H8E/N29R/T34E, is more stable than the wild-type protein by 5.6 °C in T_m and 4.7 kJ/mol in $\Delta G(H_2O)$ supports this possibility.

It is noted that the difference in stability between MR-1 and *E. coli* RNases HI is larger than that between MR-1 RNase HI and H8E/N29R/T34E by 4-fold in T_m and 3-fold in $\Delta G(H_2O)$. These results indicate that the three amino acid substitutions at the sites mentioned above account for one-third to one-fourth of the difference in stability between MR-1 and *E. coli* RNases HI. Therefore, other factors, such as an increase in the fraction of nonpolar surface area, may also contribute to the thermolability of MR-1 RNase HI.

Thermodynamic Parameters of MR-1 RNase HI. The optimum temperature of MR-1 RNase HI for activity and its stability against heat inactivation were lower than those of *E. coli* RNase HI by 10 and 19 °C, respectively, indicating that MR-1 RNase HI is thermolabile compared to *E. coli* RNase HI. Because of the thermolability and low optimum temperature for activity, MR-1 RNase HI can be defined as a cold-adapted enzyme.

Comparison of the temperature dependencies of the $\Delta G(H_2O)$ values for MR-1 and *E. coli* RNases HI indicates that MR-1 RNase HI is less stable than *E. coli* RNase HI by 12−14 kJ/mol at any temperature that was examined (Figure 10). The maximal stability, $\Delta G(T_s)$, and T_m of MR-1 RNase HI are lower than those of *E. coli* RNase HI by 12.6 kJ/mol and 17.5 °C, respectively, while the temperature for maximal stability, T_s, of MR-1 RNase HI (18.8 °C) is comparable to that of *E. coli* RNase HI (19.9 °C). It has been reported that the $\Delta G(T_s)$ value of *T. thermophilus* RNase HI is higher than that of *E. coli* RNase HI by 5.2 kcal/mol (21.7 kJ/mol), and its T_s and T_m values are 20 and 86 °C, respectively (*9*). The $\Delta G(T_s)$ values of thermophilic, mesophilic, and psychrotrophic RNases HI are thus centered at ∼20 °C, and their entire stability curves are shifted downward in this order. Similar relationships have been reported for α-amylases from thermophiles, mesophiles, and psychrophiles (*29*). It has also been reported that thermophilic and mesophilic proteins exhibit maximal stability around room temperature (25 °C), regardless of their stability (*30*). Because MR-1 RNase HI exhibits a high degree of amino acid sequence identity to *E. coli* RNase HI and its stability can be thermodynamically analyzed, MR-1 and *E. coli* RNases HI are promising materials for the analysis of the cold adaptation mechanism of proteins.

The stability of MR-1 RNase HI (19.8 kJ/mol) at the optimum growth temperature of its host organism, $\Delta G(T_L)$, is 11.4 kJ/mol lower than that of *E. coli* RNase HI. It has been reported that the $\Delta G(T_L)$ value of *T. thermophilis* RNase HI is similar to that of *E. coli* RNase HI (*9*). It has also been reported that the $\Delta G(T_L)$ values of the thermophilic and mesophilic proteins are rather constant regardless of the optimum growth temperatures of their host organisms, as long as these proteins belong to the same family (*30*). Therefore, the $\Delta G(T_L)$ value of MR-1 RNase HI is unusually low compared to those of mesophilic and thermophilic RNase HI proteins. However, it seems too early to propose that this low $\Delta G(T_L)$ value is one of the characteristic features of psychrophilic or psychrotrophic enzymes, because of the limited information about their thermodynamic stability.

The ΔC_p value of MR-1 RNase HI is slightly but significantly higher than that of *E. coli* RNase HI by 3.4 kJ mol^{-1} K^{-1}. ΔC_p is thought to arise from the hydration of surface area that is exposed upon unfolding of protein (*31*). It has been reported that the thermodynamic stability of *T. thermophilis* RNase HI is characterized by the higher $\Delta G(H_2O)$ value and lower ΔC_p value compared to those of *E. coli* RNase HI (*9*). In addition, the fraction of nonpolar surface area increases as follows: *T. thermophilis* RNase HI < *E. coli* RNase HI < MR-1 RNase HI. Therefore, as long as the thermodynamic parameters of thermophilic, mesophilic, and psychrotrophic RNases HI are compared with one another, clear correlation was observed among ΔC_p, stability, and ASA. A similar correlation between ΔC_p and stability has been reported for thermophilic ribosomal protein L30e and its destabilized mutants, in which the charged residues are replaced with noncharged residues (*32*). A ΔC_p value of a thermophilic protein that is lower than that of a mesophilic counterpart has also been reported for phosphoglycerate kinase (*33*), cytochrome *c* (*34*), CheY (*35*), 3-isopropylmalate dehydrogenase (*36*), and the catalytic domain of cellulase (*37*). Likewise, a ΔC_p value of a psychrophilic protein that is higher than that of a mesophilic counterpart has been reported for α-amylase (*38*).

The ΔC_p value can be directly determined by differential scanning calorimetry (DSC). Therefore, to confirm the ΔC_p value determined by CD, heat-induced denaturation of MR-1 RNase HI was analyzed by DSC as described previously (*8*). However, a heat capacity curve was not obtained because the protein was aggregated to form precipitates upon thermal denaturation (data not shown). For DSC analysis, the protein concentration should be increased to approximately 1 mg/mL. MR-1 RNase HI is probably unstable in a thermally denatured form at such a high concentration.

ACKNOWLEDGMENT

The synchrotron radiation experiments were performed at beamline BL44XU in SPring-8 with the approval of the Institute for Protein Research, Osaka University (2005B6709). We thank Drs. T. Inoue and Y. Kai for their support in X-ray crystallography and helpful discussions. We also thank Dr. R. Colter for providing the *S. oneidensis* MR-1 genome and Drs. M. Morikawa and A. Mukaiyama for helpful discussions.

REFERENCES

1. Myers, C. R., and Nealson, K. H. (1988) Bacterial manganese reduction and growth with manganese oxide as the sole electron acceptor, *Science 240*, 1319−1321.
2. Heidelberg, J. F., Paulsen, I. T., Nelson, K. E., Gaidos, E. J., Nelson, W. C., Read, T. D., et al. (2002) Genome sequence of the dissimilatory metal ion-reducing bacterium *Shewanella oneidensis*, *Nat. Biotechnol. 20*, 1118−1123.
3. Abboud, R., Popa, R., Souza-Egipsy, V., Giometti, C. S., Tollaksen, S., Mosher, J. J., Findelay, R. H., and Nealson, K. H. (2005) Low-temperature growth of *Shewanella oneidensis* MR-1, *Appl. Environ. Microbiol. 71*, 811−816.
4. Morita, R. Y., and Moyer, C. L. (2000) Origin of psychrophiles, in *Encyclopedia of biodiversity* (Levin, S. A., Colwell, R., Dailey, G., Lubchenco, J., Mooney, H. A., Schulze, E. D., and Tilman, G. D., Eds.) pp 917−924, Vol. 4, Academic Press, San Diego.
5. Crouch, R. J., and Dirksen, M. L. (1982) Ribonuclease H, in *Nuclease* (Linn, S. M., and Robert, R. J., Eds.) pp 211−241, Cold Spring Harbor Laboratory Press, Plainview, NY.
6. Ohtani, N., Haruki, M., Morikawa, M., and Kanaya, S. (1999) Molecular diversities of RNases H, *J. Biosci. Bioeng. 88*, 12−19.
7. Kanaya, S. (1998) Enzymatic activity and protein stability of *E. coli* ribonuclease HI, in *Ribonucleases H* (Crouch, R. J., and Toulme, J. J., Eds.) pp 1−38, INSERM, Paris.

8. Mukaiyama, A., Takano, K., Haruki, M., Morikawa, M., and Kanaya, S. (2004) Kinetic robust monomeric protein from a hyperthermophile, *Biochemistry 43*, 13859−13866.
9. Hollien, J., and Marqusee, S. (1999) A thermodynamic comparison of mesophilic and thermophilic ribonucleases H, *Biochemistry 38*, 3831−3836.
10. Smalas, A. O., Leiros, H. K., Os, V., and Willassen, N. P. (2000) Cold adapted enzymes, *Biotechnol. Annu. Rev. 6*, 1−57.
11. Gianese, G., Bossa, F., and Pascarella, S. (2002) Comparative structural analysis of psychrophilic and meso- and thermophilic enzymes, *Proteins 47*, 236−249.
12. Feller, G., and Gerday, C. (2003) Psychrophilic enzymes: Hot topics in cold adaptation, *Nat. Rev. Microbiol. 1*, 200−208.
13. Siddiqui, K. S., and Cavicchioli, R. (2006) Cold-adapted enzymes, *Annu. Rev. Biochem. 75*, 403−433.
14. Ohtani, N., Haruki, M., Morikawa, M., and Kanaya, S. (2001) Heat labile ribonuclease HI from a psychrotrophic bacterium: Gene cloning, characterization and site-directed mutagenesis, *Protein Eng. 14*, 975−982.
15. Kanaya, S., Katsuda, C., Kimura, S., Nakai, T., Kitakuni, E., Nakamura, H., Katayanagi, K., Morikawa, K., and Ikehara, M. (1991) Stabilization of *Escherichia coli* ribonuclease H by introduction of an artificial disulfide bond, *J. Biol. Chem. 266*, 6038−6044.
16. Laemmli, U. K. (1970) Cleavage of structural proteins during assembly of the head of bacteriophage T4, *Nature 227*, 680−685.
17. Goodwin, T. W., and Morton, R. A. (1946) The spectrophotometric determination of tyrosine and tryptophan in proteins, *Biochem. J. 40*, 628−630.
18. Otwinowski, Z., and Minor, W. (1997) Processing of X-ray diffraction data collected in oscillation mode, *Methods Enzymol. 276*, 307−326.
19. Vagin, A., and Teplyakov, A. (1997) MOLREP: An automated program for molecular replacement, *J. Appl. Crystallogr. 30*, 1022−1025.
20. Emsley, P., and Cowtan, K. (2004) *Coot*: Model-building tools for molecular graphics, *Acta Crystallogr. D60*, 2126−2132.
21. Murshudov, G. N., Vagin, A. A., and Dodson, E. J. (1997) Refinement of macromolecular structures by the maximum-likelihood method, *Acta Crystallogr. D53*, 240−255.
22. Laskowski, R. A., MacArthur, M. W., Moss, D. S., and Thornton, J. M. (1993) PROCHECK: A program to check the stereochemical quality of protein structures, *J. Appl. Crystallogr. 26*, 283−291.
23. Sayle, R. A., and Milner-White, E. J. (1995) RASMOL: Biomolecular graphics for all, *Trends Biochem. Sci. 20*, 374.
24. Collaborative Computational Project, Number 4 (1994) The CCP4 suite: Programs for protein crystallography, *Acta Crystallogr. D50*, 760−763.
25. Nicholls, A., Sharp, K., and Honig, B. (1991) Protein folding and association: Insights from the interfacial and thermodynamic properties of hydrocarbons, *Proteins: Struct., Funct., Genet. 11*, 281−296.
26. Pace, C. N. (1990) Measuring and increasing protein stability, *Trends Biotechnol. 8*, 93−98.
27. Arnorsdottir, J., Kristjansson, M. M., and Ficner, R. (2005) Crystal structure of a subtilisin-like serine proteinase from a psychrotrophic *Vibrio* species reveals structural aspects of cold adaptation, *FEBS J. 272*, 832−845.
28. Bae, E., and Phillips, G. N., Jr. (2004) Structures and analysis of highly homologous psychrophilic, mesophilic, and thermophilic adenylate kinases, *J. Biol. Chem. 279*, 28202−28208.
29. D'Amico, S., Marx, J. C., Gerday, C., and Feller, G. (2003) Activity-stability relationships in extremephilic enzymes, *J. Biol. Chem. 278*, 7891−7896.
30. Kumer, S., Tsai, C. J., and Nussinov, R. (2001) Thermodynamic difference among thermophilic and mesophilic proteins, *Biochemistry 40*, 14152−14165.
31. Gomez, J., Hilser, V. J., Xie, D., and Freire, E. (1995) The heat capacity of proteins, *Proteins: Struct., Funct., Genet. 22*, 404−412.
32. Lee, C.-F., Allen, M. D., Bycroft, M., and Wong, K. B. (2005) Electrostatic interactions contribute to reduced heat capacity change of unfolding in a thermophilic ribosomal protein L30e, *J. Mol. Biol. 348*, 419−431.
33. Grattinger, M., Dankesreiter, A., Schurig, H., and Jaenicke, R. (1998) Recombinant phosphoglycerate kinase from the hyperthermophilic bacterium *Thermotoga maritima*: Catalytic, spectral and thermodynamic properties, *J. Mol. Biol. 280*, 525−533.
34. Uchiyama, S., Hasegawa, J., Tanimoto, Y., Moriguchi, H., Mizutani, M., Igarashi, Y., Sambongi, Y., and Kobayashi, Y. (2002) Thermodynamic characterization of variants of mesophilic cytochrome c and its thermophilic counterpart, *Protein Eng. 15*, 455−462.
35. Deutschman, W. A., and Dahlquist, F. W. (2001) Thermodynamic basis for the increased thermostability of CheY from the hyperthermophile *Thermotoga maritima*, *Biochemistry 40*, 13107−13113.
36. Motono, C., Oshima, T., and Yamagishi, A. (2001) High thermal stability of 3-isopropylmalate dehydrogenase from *Thermus thermophilus* resulting from low ΔC_p of unfolding, *Protein Eng. 14*, 961−966.
37. Beadle, B. M., Baase, W. A., Wilson, D. B., Gilkes, N. R., and Shoichet, B. K. (1999) Comparing the thermodynamic stabilities of a related thermophilic and mesophilic enzyme, *Biochemistry 38*, 2570−2576.
38. Feller, G., d'Amico, D., and Gerday, C. (1999) Thermodynamic stability of a cold-active α-amylase from the Antarctic bacterium *Alteromonas haloplanctis*, *Biochemistry 38*, 4613−4619.

BI7001423